Perturbation dynamics in viscous channel flows

By W. O. CRIMINALE[1], T. L. JACKSON[2],
D. G. LASSEIGNE[3] AND R. D. JOSLIN[4]

[1]Department of Applied Mathematics, University of Washington, Seattle, WA 98195, USA

[2]Institute for Computer Applications in Science and Engineering,
NASA Langley Research Center, Hampton, VA 23681-0001, USA

[3]Department of Mathematics and Statistics, Old Dominion University, Norfolk, VA 23529, USA

[4]NASA Langley Research Center, Hampton, VA 23681-0001, USA

Plane viscous channel flows are perturbed and the ensuing initial-value problems are investigated in detail. Unlike traditional methods where travelling wave normal modes are assumed as solutions, this work offers a means whereby arbitrary initial input can be specified without having to resort to eigenfunction expansions. The full temporal behaviour, including both early-time transients and the long-time asymptotics, can be determined for any initial small-amplitude three-dimensional disturbance. The bases for the theoretical analysis are: (*a*) linearization of the governing equations; (*b*) Fourier decomposition in the spanwise and streamwise directions of the flow; and (*c*) direct numerical integration of the resulting partial differential equations. All of the stability criteria that are known for such flows can be reproduced. Also, optimal initial conditions measured in terms of the normalized energy growth can be determined in a straightforward manner and such optimal conditions clearly reflect transient growth data that are easily determined by a rational choice of a basis for the initial conditions. Although there can be significant transient growth for subcritical values of the Reynolds number, it does not appear possible that arbitrary initial conditions will lead to the exceptionally large transient amplitudes that have been determined by optimization of normal modes when used without regard to a particular initial-value problem. The approach is general and can be applied to other classes of problems where only a finite discrete spectrum exists (e.g. the Blasius boundary layer). Finally, results from the temporal theory are compared with the equivalent transient test case in the spatially evolving problem with the spatial results having been obtained using both a temporally and spatially accurate direct numerical simulation code.

1. Introduction

The subject of the fate of disturbances in well-established shear flows remains a major topic of fluid mechanics. As the means of obtaining quantitative results for any specific problem has improved, the number of contributions in this area has grown almost without bounds. And, indeed, almost every conceivable prototypical flow has been subjected to scrutiny in this manner. The scheme is well conceived: introduce perturbations into a defined basic flow, linearize the governing equations, and then determine from the initial-value problem the resulting dynamics. In principle this can be done but, in practice, it is a formidable task. Difficulties entail non-self-adjoint and singular differential equations among other obstacles. Even the use of the computer

and numerical methods have not been easily adaptable. Thus, the net result is that (almost without exception) it was considered adequate if a flow was determined to be asymptotically stable or unstable. This was done by assuming a separable normal mode solution in the form of travelling waves and then establishing the existence of at least one unstable eigenvalue. No attention was directed to any particular initial value or the transient period of the dynamics. Indeed, this part of the evolution was not thought to have any significance and, in view of the complications involved in the linear ordinary differential equations, it was left to speculation.

More recently the early transient period for the perturbations has been shown to reveal that a superposition of decaying normal modes may grow initially, but decay as time goes on. Although the basic origins and recognition of this type of response should properly be ascribed to Kelvin (1887) and Orr (1907*a, b*), there is an ever widening development, see Boberg & Brosa (1988), Gustavsson (1991), Butler & Farrell (1992), Reddy & Henningson (1993), or Trefethen *et al.* (1993) as major references. Briefly, it has been shown that transient growth can be significant even for subcritical values of the Reynolds number and therefore nonlinearity may ensue, making an exponentially growing normal mode a moot point. In point of fact, this sort of behaviour is not hard to grasp because any non-self-adjoint differential equation will have eigenfunctions that are not orthogonal and therefore there can be algebraic behaviour for early time (see Sommerfeld 1949). It is also clear that the least-damped normal modes should be the ones that are dominant during this early period.

Other approaches for demonstrating algebraic growth of perturbations have been given by Gustavsson (1979), Hultgren & Gustavsson (1980), Benney & Gustavsson (1981), and Criminale & Drazin (1990). In the first case, Laplace transforms were used for solving the disturbance equations and algebraic behaviour was found because branch cuts are needed for the inversion of the transforms; poles correspond to exponential growth or decay. Benney & Gustavsson (1981) have shown that, if three-dimensional disturbances are considered, then there can be a resonance between the normal modes of the Orr–Sommerfeld equation and those of the Squire equation. Such resonance does occur and it is for damped exponential modes. The last paper dealt with the existence of the continuous spectrum as well as the discrete normal modes using yet another approach but, again, it is algebraic temporal behaviour that results. The Laplace inversions that led to algebraic growth were also due to the continuous rather than the discrete spectrum but, unlike the Criminale & Drazin presentation, general initial values were not taken into account.

The results of the various investigations that have been made for channel flows suggest that the early transient growth can be extremely large (factors of 20 to 1000) at subcritical values of the Reynolds number when considering optimal growth measured in terms of normalized kinetic energy growth determined from variational techniques. It should be emphasized that not one exponentially growing mode is involved in this process. One may ask whether this exceptional growth for an optimal disturbance would occur regardless of the initial input. Granted, variational calculations will assign values to the coefficients of the modes of the expansion in terms of the eigenfunctions, but such a determination may not be the same as for a *specific* initial-value distribution used to determine the relative values of the coefficients of the eigenmodes. As outlined in Betchov & Criminale (1967) and Drazin & Reid (1981), the use of the eigenfunctions in the initial-value problem requires the solution of the adjoint differential equation in order to establish the values of the coefficients. Moreover, it is known from Schensted (1960) that the set of such functions is complete for channel flows and consequently there is no conceptual difficulty in the

prescription. Also, there is no continuous eigenspectrum for viscous channel flows. Thus, transient growth in channel flows is due entirely to the non-orthogonality of the eigenfunctions of the non-self-adjoint differential equations and the resonance between Orr–Sommerfeld and Squire discrete modes.

The optimal formulation is due to Farrell (1988) and Butler & Farrell (1992)† and has been independently corroborated by Reddy & Henningson (1993). Up to thirty eigenmodes were employed in these works with relative amplitudes ranging from order one to one thousand. Typically, the normalized kinetic energy of the perturbations as a function of time showed that transient growth can lead to the large amplitudes cited before there is eventual decay. The initial distributions used for the optimal values are given in Farrell (1988) and Butler & Farrell (1992). In terms of the initial-value problem this is important information and certainly bears heavily on the possible physical realization. Examination of the initial conditions that produce optimal growth show that the optimal initial conditions for strictly two-dimensional disturbances have discernible structure while those that produce optimal growth of three-dimensional disturbances are rather nondescript. Thus it should be relatively easy to choose initial conditions that approximate the three-dimensional optimal conditions while some care must be taken to choose initial conditions that will approximate the optimal two-dimensional disturbance. The study of the possible realization of the optimal conditions is a major point of this work. Butler & Farrell (1994) show that a threshold amplitude exists for optimally configured two-dimensional initial conditions. For amplitudes above the threshold, transient growth leads to a nonlinear evolution to quasi-steady finite-amplitude structures and for amplitudes below the threshold, the decay rate for long-time behaviour is predicted by the slowest decaying Orr–Sommerfeld mode. The optimization procedures using the eigenfunction expansions in these studies are dependent on the fact that the discrete eigenfunctions form a complete set and therefore are not directly applicable to a problem such as the Blasius boundary layer where the complete set was shown by Salwen & Grosch (1981) to be a linear combination of discrete *and* continuum eigenfunctions. Butler & Farrell (1992) did study the Blasius boundary layer optimization problem by using the channel flow solutions to represent the continuous spectrum as a discrete set of modes. Thus, the initial transient to disturbances which decay exponentially in the free stream was determined, but finiteness of the perturbations in the free stream was not considered and hence is not a good approximation to the continuous spectrum. The solution procedure chosen here does not present the same difficulties in generalization to a problem with a continuous spectrum since it does not depend on the expansion of an initial condition in terms of eigenfunctions.

The presentation of Gustavsson (1991) was somewhat different in that one normal mode from the Orr–Sommerfeld equation was combined with six modes of the accompanying Squire equation. In effect, this is an initial-value problem. Similarly, a measure of the energy is displayed but with the concentration on the energy gained by the Squire mode. The unknown coefficients were determined by requiring the Orr–Sommerfeld mode to have an energy of unity at time zero. It was shown that, if there is sufficient obliquity of the waves (nearly 90°), the energy for the Squire mode can transiently increase by a factor of almost 100. In this case, three-dimensionality is crucial but this in no way makes it accessible as a method for realizing large transient

---

† Farrell & Moore (1992) also integrated the governing equations for oceanic flows, but again their focus was on determining an optimal initial condition by repeated integration of the perturbation equations and its adjoint and not on the dynamics of specific initial conditions.

growth in an arbitrary initial-value problem. Gustavsson did consider the effects of symmetrical and asymmetrical superposition of the two sets of eigenfunctions and there are decidedly different responses depending upon which choice is made. In particular, a symmetric Orr–Sommerfeld mode interacting with an asymmetrical Squire mode leads to the largest amplitude for the energy. In every case, there is eventual decay after the maximum as time advances for subcritical values of the Reynolds numbers.

Like the Blasius boundary layer, viscosity is critical to the perturbations in channel flows. Without a viscous fluid, there is no instability in any of these flows when cast in terms of normal modes. Case (1960) investigated plane Couette flow in an inviscid fluid and demonstrated by using Laplace transforms in time that there are no normal modes at all, whether decaying or growing. At the same time he also showed that there are other solutions to this problem if one makes the proper analysis. The additional solutions are those due to a continuous eigenspectrum. Although not covered to this extent, plane Poiseuille flow must follow in like manner. Once the fluid is viscous, then the results are reversed, i.e. there is no continuous spectrum for channel flows but it has been proven that there is an infinite number of normal modes and the set is complete (Schensted 1960; DiPrima & Habetler 1969). The Blasius boundary layer (e.g. Gustavsson 1979) possesses both spectra because it is a semi-infinite problem. Parenthetically, it is interesting to note that there is only a *finite* number of normal modes for the Blasius boundary layer however (see Mack 1976; Grosch & Salwen 1978), with the number depending upon the value of the Reynolds number. Salwen & Grosch (1981) showed how an arbitrary initial disturbance could be expanded in terms of the complete set of discrete and continuum eigenfunctions but determining an optimal initial condition would be difficult. For infinite Reynolds number there may exist an infinite set of normal modes that are either damped or neutral.

Physically, viscosity causes instability in much the same way that a spring would be unstable if the spring force had a time delay. Mathematically, it is a question of a phase shift between the perturbations. This is best illustrated by considering the equation for the total kinetic energy of the perturbations. The time rate of change for this energy depends upon two essential terms: dissipation due to viscosity and production manifested by one of the Reynolds stress components interacting with the mean flow to transfer energy and overcome the viscous dissipation. In terms of normal modes, the latter process is possible for Poiseuille but not for Couette flow. And, the Blasius boundary layer is also unstable in these terms. In terms of the energy, all shear flows can be examined in this fashion but, of the flows unstable because of viscosity, only plane Poiseuille flow and the boundary layer are unstable asymptotically. Plane Couette flow lacks the critical phase shift due to the fact that there is no gradient of the mean vorticity (cf. Betchov & Criminale 1967 and Drazin & Reid 1981).

Because of the Squire theorem and the fact that a stability boundary was desired, three-dimensionality *per se* was neglected because it was recognized that purely two-dimensional disturbances had the largest growth factors. Another often overlooked point is the fact that the Orr–Sommerfeld equation is only fourth rather than sixth order. This result is fortuitous, makes for ease in the mathematics, but omits important physics. The resolution of this problem is the Squire mode equation that is coupled to the behaviour of the Orr–Sommerfeld equation so long as there is three-dimensionality. It is this pair of governing equations that has formed the basis for the cited studies in transient temporal behaviour. Except for the investigations that use the Laplace transforms for the Blasius boundary layer, the work has relied

almost completely on solutions in terms of normal modes. As is the theme of this work, Bruer & Kuraishi (1994) integrated the partial differential equation considering a special initial disturbance for the boundary layer. However, the transient dynamics were not considered closely. If the transient dynamics are to be important, then the effects of specific initial conditions must be examined together with any optimum strategy. Certainly, three-dimensionality must be treated in a thorough manner.

The determination of the dynamics of the linear perturbation problem is the central goal of this presentation. This is done with the use of numerical integration of the governing partial differential equations. In no way is an expansion in normal modes suggested but, at the same time, it will be seen that all of the known results of classical stability theory as well as the optimization problem can be addressed. The details of the perturbation field, most notably the inclusion of a vorticity component, in the initial conditions are found to greatly affect the achievement of large transient growth in terms of the normalized energy. The basic problem is formulated in §2, and the numerical method is outlined in §3. Section 4 presents results in terms of a normalized perturbation energy for two- and three-dimensional disturbances, as well as a presentation of optimal initial conditions. Results from the temporal theory are compared with the equivalent transient test case in the spatially evolving problem in §5. For the spatial results, a temporally and spatially accurate direct numerical simulation code is employed. A description of the code is also presented in §5. Finally, conclusions are given in §6.

2. Basic governing equations

The fluid is taken as incompressible with a parallel base flow $U = U(y), V = W = 0$. Then, the non-dimensional linearized equations of motion can be written, with u, v, w the perturbation velocity components in the x, y, z directions and p the perturbation pressure, as

$$\frac{\partial u}{\partial x} + \frac{\partial v}{\partial y} + \frac{\partial w}{\partial z} = 0, \tag{1}$$

$$\frac{\partial u}{\partial t} + U\frac{\partial u}{\partial x} + \frac{dU}{dy}v + \frac{\partial p}{\partial x} = Re^{-1}\left[\frac{\partial^2 u}{\partial x^2} + \frac{\partial^2 u}{\partial y^2} + \frac{\partial^2 u}{\partial z^2}\right], \tag{2}$$

$$\frac{\partial v}{\partial t} + U\frac{\partial v}{\partial x} + \frac{\partial p}{\partial y} = Re^{-1}\left[\frac{\partial^2 v}{\partial x^2} + \frac{\partial^2 v}{\partial y^2} + \frac{\partial^2 v}{\partial z^2}\right], \tag{3}$$

and

$$\frac{\partial w}{\partial t} + U\frac{\partial w}{\partial x} + \frac{\partial p}{\partial z} = Re^{-1}\left[\frac{\partial^2 w}{\partial x^2} + \frac{\partial^2 w}{\partial y^2} + \frac{\partial^2 w}{\partial z^2}\right]. \tag{4}$$

Here, $Re = U_o h/v$ is the Reynolds number, where h is the channel half-width, U_o the centreline velocity and v the kinematic viscosity. Time is non-dimensionalized by the advective time scale h/U_o. On using the Fourier transformations defined with respect to x and z as

$$\check{v}(\alpha; y; \gamma; t) = \int_{-\infty}^{\infty}\int_{-\infty}^{\infty} v(x, y, z, t)e^{i(\alpha x + \gamma z)}dxdz, \tag{5}$$

where α and γ are taken to be real and are the non-dimensional wavenumbers in the x- and z-directions, respectively, equations (1) to (4) become

$$-i(\alpha\check{u} + \gamma\check{w}) + \frac{\partial\check{v}}{\partial y} = 0, \tag{6}$$

$$\frac{\partial \breve{u}}{\partial t} - i\alpha U\breve{u} + U'\breve{v} - i\alpha\breve{p} = Re^{-1}\left[\frac{\partial^2 \breve{u}}{\partial y^2} - \tilde{\alpha}^2\breve{u}\right], \tag{7}$$

$$\frac{\partial \breve{v}}{\partial t} - i\alpha U\breve{v} + \frac{\partial \breve{p}}{\partial y} = Re^{-1}\left[\frac{\partial^2 \breve{v}}{\partial y^2} - \tilde{\alpha}^2\breve{v}\right], \tag{8}$$

and

$$\frac{\partial \breve{w}}{\partial t} - i\alpha U\breve{w} - i\gamma\breve{p} = Re^{-1}\left[\frac{\partial^2 \breve{w}}{\partial y^2} - \tilde{\alpha}^2\breve{w}\right], \tag{9}$$

with $U' = dU/dy$ and $\tilde{\alpha}^2 = \alpha^2 + \gamma^2$.

The Squire transformation, written as

$$\alpha\breve{u} + \gamma\breve{w} = \tilde{\alpha}\tilde{u}, \tag{10}$$

$$-\gamma\breve{u} + \alpha\breve{w} = \tilde{\alpha}\tilde{w}, \tag{11}$$

and combined with operations on (6) to (9) enables us to obtain the pair of equations

$$\left[\frac{\partial}{\partial t} - i\alpha U\right]\left(\frac{\partial^2 \breve{v}}{\partial y^2} - \tilde{\alpha}^2\breve{v}\right) + i\alpha U''\breve{v} = Re^{-1}\left[\frac{\partial^4 \breve{v}}{\partial y^4} - 2\tilde{\alpha}^2\frac{\partial^2 \breve{v}}{\partial y^2} + \tilde{\alpha}^4\breve{v}\right] \tag{12}$$

and

$$\left[\frac{\partial}{\partial t} - i\alpha U\right]\tilde{w} = \sin\phi U'\breve{v} + Re^{-1}\left[\frac{\partial^2 \tilde{w}}{\partial y^2} - \tilde{\alpha}^2\tilde{w}\right] \tag{13}$$

where $\sin\phi = \gamma/\tilde{\alpha}$ and $\tilde{w}$ is proportional to the normal vorticity component ($\breve{\omega}_y = i\tilde{\alpha}\tilde{w}$). The first term on the right-hand side of (13) is known as the vortex tilting term and acts as forcing for the normal vorticity component. The vortex tilting term is a product of the mean vorticity in the spanwise direction ($\Omega_z = -U'$) and the perturbation strain rate ($\partial v/\partial z$) and, for a three-dimensional disturbance, gives rise to the increase of the normal vorticity. It is clear that the solutions of (12) and (13) combined with continuity and the Squire transformation are equivalent to solving (6) to (9). Likewise, $\breve{p}$ can be determined from (9). In either case, solutions of the equations are subject to imposed initial conditions and the following boundary conditions at the channel walls:

$$\breve{v}(\pm 1, t) = \frac{\partial \breve{v}}{\partial y}(\pm 1, t) = \tilde{w}(\pm 1, t) = 0. \tag{14}$$

For the mean velocity, we shall consider both plane Poiseuille flow where

$$U(y) = 1 - y^2$$

and plane Couette flow where

$$U(y) = y.$$

To evaluate the other velocity components, the quantities $\breve{v}$ and $\tilde{w}$ are first computed from (12) and (13), respectively. Then the Squire transformation, (10) and (11), when combined with (6) can be inverted to give

$$\breve{u} = -\frac{i\cos\phi}{\tilde{\alpha}}\frac{\partial \breve{v}}{\partial y} - \sin\phi\tilde{w}, \tag{15}$$

and

$$\breve{w} = -\frac{i\sin\phi}{\tilde{\alpha}}\frac{\partial \breve{v}}{\partial y} + \cos\phi\tilde{w}. \tag{16}$$

By knowing the velocity, the vorticity perturbations can be determined in a straightforward manner by appealing to the definitions, namely

$$\breve{\omega}_x = \frac{\partial \breve{w}}{\partial y} + \mathrm{i}\gamma\breve{v}, \tag{17}$$

$$\breve{\omega}_y = -\mathrm{i}\gamma\breve{u} + \mathrm{i}\alpha\breve{w} \equiv \mathrm{i}\tilde{\alpha}\breve{w}, \tag{18}$$

and

$$\breve{\omega}_z = -\mathrm{i}\alpha\breve{v} - \frac{\partial \breve{u}}{\partial y}. \tag{19}$$

Finally, we remark here that, if one seeks solutions to (12) and (13) of the form $\mathrm{e}^{-\mathrm{i}\omega t}$, then (12) and (13) become the more familiar Orr–Sommerfeld and Squire equations. Solutions of these equations will yield classical normal modes and usually transient dynamics and the effects of various initial conditions are ignored. At subcritical Reynolds numbers, where normal modes are damped, the transient behaviour may be extremely important. A variety of authors have used eigenfunction expansions to examine transients (e.g. Gustavsson 1991; Butler & Farrell 1992; Reddy & Henningson 1993 as principal references). In particular, since the eigenfunctions form a complete set (DiPrima & Habetler 1969; Herron 1980), solutions to (12) and (13) were sought in the form

$$\left[\begin{array}{c} \breve{v}(y,t) \\ \breve{w}(y,t) \end{array} \right] = \sum_j A_j \mathrm{e}^{-\mathrm{i}\lambda_j t} \left[\begin{array}{c} v_j(y) \\ w_j^p(y) \end{array} \right] + \sum_j B_j \mathrm{e}^{-\mathrm{i}\mu_j t} \left[\begin{array}{c} 0 \\ w_j(y) \end{array} \right],$$

where $\{\lambda_j\}$ and $\{\mu_j\}$ are the eigenvalues of the Orr–Sommerfeld and Squire equations, respectively, with the eigenvalues distinct; A_j, B_j are arbitrary constants to be determined by initial conditions, and w_j^p are the particular solutions to the Squire equation; v_j and w_j are the respective homogeneous solutions. As already noted, either (i) variational methods are then used to determine optimal growth; or (ii) a finite combination of eigenfunctions, though limited, is then chosen and the subsequent transient behaviour followed. This is not necessarily a weakness because an infinite set is available but to date has been limited to the use of only a finite number. An alternative approach is to solve the system (12) and (13) directly by a numerical scheme. While this approach does not directly select the optimal initial conditions that provide the optimal algebraic growth for a given set of parameters $(\tilde{\alpha}, \phi, Re)$, it does allow one to follow rather easily the transient dynamics of an arbitrarily prescribed initial condition and to determine if optimal growth can be approximated by such realizable initial conditions. Also, maximization methods (see §4.3) can be easily applied to the numerical solution in order to select the optimal initial condition. Here we show a method to find the optimal condition that circumvents the necessity of using the adjoint solution and is conceptionally easy to understand and implement. Finally, this approach is more robust than employing eigenfunction expansions since it can be applied to other classes of problems where only a finite number of normal modes exist, e.g. boundary layers, free shear layers (see Criminale, Jackson & Lasseigne 1995 for related work on inviscid flows).

3. Numerical solutions

The partial differential equations (12) and (13) were solved numerically by the method of lines (see Ames 1977). The spatial derivatives were centre differenced on

Grid points	Growth rate
500	0.003726
1000	0.003736
2000	0.003739

TABLE 1. Numerically computed temporal growth rate for plane Poiseuille flow as a function of grid points.
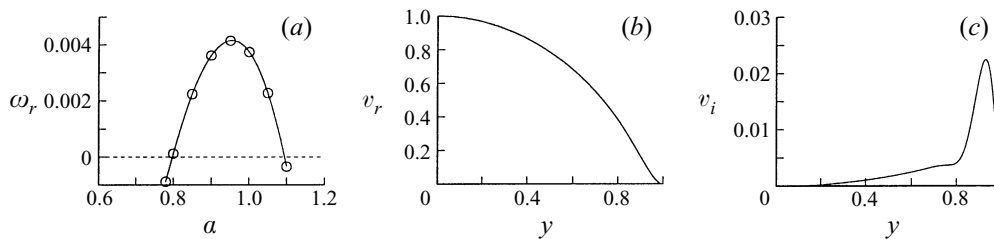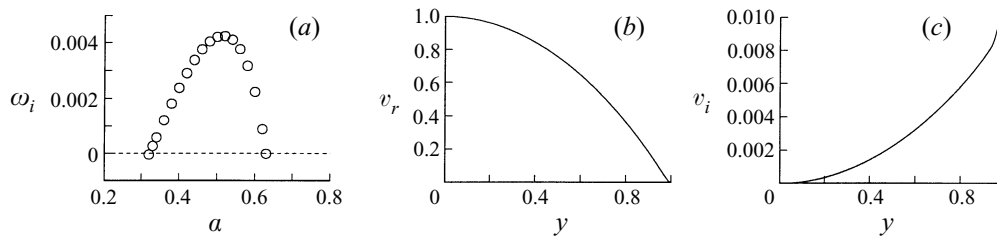

FIGURE 1. (*a*) Growth rates as a function of wavenumber α. The circles correspond to the numerically computed values from the partial differential equation, and the solid curve corresponds to the growth rate computed using the Orr–Sommerfeld equation. (*b*) The real part and (*c*) the imaginary part of the eigenfunction as a function of y for $\alpha = 1$. Results for plane Poiseuille flow with $\phi = 0°$ and $Re = 10^4$.

FIGURE 2. (*a*) Growth rates as a function of wavenumber α. The circles correspond to the numerically computed values from the partial differential equation. (*b*) The real part and (*c*) the imaginary part of the eigenfunction as a function of y for $\alpha = 0.44$. Results for plane Poiseuille flow with $\phi = 0°$ and $Re = 10^6$.

a uniform grid within the channel while one-sided differences were used at the walls. The resulting system was then integrated in time by a fourth-order Runge–Kutta scheme with all calculations done in 64-bit precision. The results were checked for convergence by increasing the number of mesh points, varying between 500 for low Reynolds numbers to a maximum of 10 000 at larger Reynolds numbers. Table 1 shows the numerically computed temporal growth rate for plane Poiseuille flow as a function of grid points for $Re = 10\,000$, $\tilde{\alpha} = 1$ and $\phi = 0°$. A more exact value given by Orszag (1971) is 0.00373967. In any case, the number of grid points was sufficient to resolve the boundary layers near the walls but no effort was made to optimize the number of grid points by employing non-uniform meshes. If this were done, far fewer grid points would be needed. All calculations presented in this paper represent converged solutions.

Before investigating the effects of various initial conditions and their subsequent transient behaviour, it was first instructive to compare the numerically computed

growth rates and eigenfunctions for plane Poiseuille flow to those using the Orr–Sommerfeld equation at super-critical Reynolds numbers. Figure 1(*a*) shows the growth rates obtained from the numerical solution of (12) (shown as circles) and those obtained from the Orr–Sommerfeld equation (shown as the solid curve) for $Re = 10\,000$ and $\phi = 0°$. The agreement is excellent. The corresponding real and imaginary parts of the eigenfunctions from both the numerical solution (solid) and the Orr–Sommerfeld solution (dashed) are displayed in figures 1(*b*) and 1(*c*), respectively, for the case $\tilde{\alpha} = 1$ and $\phi = 0°$. Note that the two curves essentially lie on top of each other. To demonstrate the strength of the procedure, figure 2 shows similar results but at $Re = 10^6$; in this case no comparative calculations have been reported.

4. Perturbation energy

As mentioned above, we are particularly interested in the effects of various initial conditions and their subsequent transient behaviour at subcritical Reynolds numbers. In order to examine the evolution of various initial conditions, the energy density in the $(\tilde{\alpha}, \phi)$-plane as a function of time is computed. The energy density is defined as

$$E(t; \tilde{\alpha}, \phi, Re) = \int_{-1}^{1} \left[|\check{u}^2| + |\check{v}^2| + |\check{w}^2| \right] \mathrm{d}y. \tag{20}$$

The total energy of the perturbation can be found by integrating (20) over all $\tilde{\alpha}$ and ϕ. A growth function can be defined in terms of the normalized energy density, namely

$$G(t; \tilde{\alpha}, \phi, Re) = \frac{E(t; \tilde{\alpha}, \phi, Re)}{E(0; \tilde{\alpha}, \phi, Re)} \tag{21}$$

measures the growth in energy at time t for a prescribed initial condition at $t = 0$.

Various initial conditions are used to explore transient behaviour at subcritical Reynolds numbers with the important issue here being the ability to make, in a simple manner, arbitrary specifications. Since a normal mode decomposition provides a complete set of eigenfunctions, it is true that any arbitrary specification can (theoretically) be written in terms of an eigenfunction expansion. However, there is nothing special about the eigenfunctions when it comes to specifying initial conditions, but they do represent the most convenient means of specifying the long-time solution. In addition, the use of the (non-orthogonal) eigenfunctions in the attempt to make any truly arbitrary specification introduces unnecessary mathematical complications which actually involve tedious numerical calculations. Physically, it would seem that the natural issues affecting the initial specification are whether the disturbances being considered are (*a*) symmetric or antisymmetric and (*b*) local or more diffuse across the channel. The cases listed below satisfy both of these needs and use functions that can be definitively employed to represent any arbitrary initial distribution. This approach, of course, offers a complete departure from the specification of the initial conditions using normal mode decomposition, but, as previously stated, the use of an eigenfunction expansion to address the natural issues affecting arbitrary initial disturbances is mathematically infeasible. The remaining salient question is whether or not the large optimal transient growth previously determined can be realized at all by an arbitrarily specified initial condition (which is the only kind of disturbance which occurs naturally in an unforced environment). The analysis presented in this section clearly shows what properties the initial condition must have in order to produce significant growth. Furthermore, it should be asked whether or not the basis functions used for the expansion of the initial conditions have any predictive

Case	$\check{v}(y,0)$
I	$\Omega_0(1-y^2)^2$
II	$(\Omega_0/\beta^2)[\cos\beta - \cos(\beta y)]; \quad \beta = n\pi$
III	$(\Omega_0/\beta^2)[\cos\beta - \cos(\beta y)]\mathrm{e}^{-y^2/4\lambda}/(4\pi\lambda)^{1/2}; \quad \beta = n\pi$
IV	$\Omega_0 y(1-y^2)^2$
V	$(\Omega_0/\beta^2)[\cos\beta - \cos(\beta y)]y\mathrm{e}^{-y^2/4\lambda}/(4\pi\lambda)^{1/2}; \quad \beta = n\pi$

TABLE 2. Initial conditions for $\check{v}$ for the integration of (12).

Case	$\tilde{w}(y,0)$
i	0
ii	$\Omega_1\cos(\beta_0 y); \quad \beta_0 = (2n-1)\pi/2$
iii	$\Omega_1\sin(\beta_1 y); \quad \beta_1 = n\pi$

TABLE 3. Initial conditions for $\tilde{w}$ for the integration of (13).

properties that can be exploited *a priori* in determining the optimal conditions. Because of the temporal dependence of the eigenfunctions, any eigenfunction taken individually does not provide any clues as to its importance in a calculation of optimal conditions; furthermore, some of the eigenfunctions are nearly linearly dependent in a spatial sense which can further cloud the issue of their importance. After identifying the initial conditions (from the cases listed below) that are the most relevant to transient growth, a straightforward optimization procedure is used to show that the results of the transient calculations performed do indeed have a strong predictive property. Furthermore, the set chosen provides a complete orthogonal basis for the easy specification of arbitrary conditions.

For the integration of (12) the initial conditions for $\check{v}$ are provided in table 2; $\Omega_0 = \Omega_0(\alpha, \gamma)$ and is the Fourier transform of the x, z dependence prescribed at time $t = 0$; λ represents the degree of spread in the y-direction for these choices of initial conditions. Note that the first three cases correspond to symmetric initial conditions while the last two are asymmetric. For the integration of (13) the initial conditions for $\tilde{w}$ are provided in table 3; $\Omega_1 = \Omega_1(\alpha, \gamma)$ and is again the Fourier transform of the x, z dependence at $t = 0$. The second initial condition is symmetric while the last is asymmetric.

4.1. *Two-dimensionality*

In this subsection results are presented for plane Poiseuille flow with $\tilde{\alpha} = 1.48$, $\phi = 0°$ and a Reynolds number of $Re = 5000$, and for plane Couette flow with $\tilde{\alpha} = 1.21$, $\phi = 0°$ and $Re = 1000$. For plane Poiseuille flow, this Reynolds number is subcritical and thus the growth function G will eventually decay in time to zero. Because plane Couette flow is linearly stable, G will always eventually decay. Then, these values correspond to those found by Butler & Farrell (1992) to be optimal for two-dimensional disturbances using variational techniques in the sense that they give the largest algebraic growth.

The growth function is plotted as a function of time in figure 3 for plane Poiseuille flow and in figure 4 for plane Couette flow. In both figures, the curves in (*a*) correspond to all possible combinations of the initial conditions for $\check{v}$ and $\tilde{w}$ given in tables 2 and 3 with $\Omega_0 = \Omega_1 = \lambda = n = 1$. (Note that the choices for $\Omega_0 = \Omega_1 = 1$ essentially means that no wavenumber is biased in the α–γ Fourier space.) Except
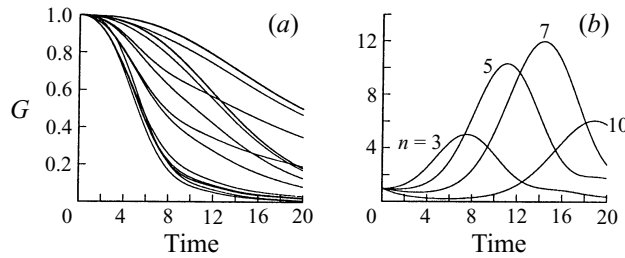
FIGURE 3. The growth function G as a function of time for various initial conditions. Results for plane Poiseuille flow with $\tilde{\alpha} = 1.48$, $\phi = 0°$, and $Re = 5000$.
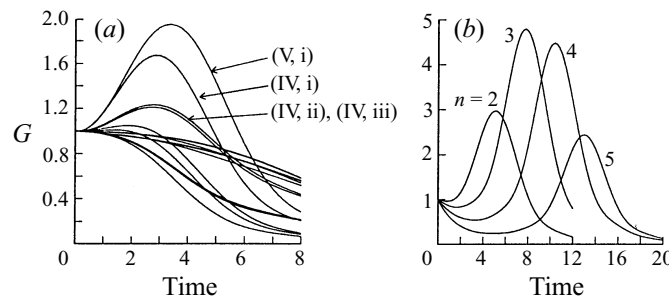

FIGURE 4. The growth function G as a function of time for various initial conditions. Results for plane Couette flow with $\tilde{\alpha} = 1.21$, $\phi = 0°$, and $Re = 1000$.

for some minor algebraic growth in the case of plane Couette flow, the growth function decays. This decrease in the amplitude of the maximum growth is somewhat unexpected since previous work shows that by considering optimal initial conditions substantial growth can occur even for these two-dimensional disturbances. Therefore, this issue was investigated further by considering initial disturbance velocity profiles with more zeros which, in some sense, corresponds to the higher eigenmodes whose inclusion in the optimization analysis was necessary to achieving the high growth rates. Figures 3(b) and 4(b) are for the initial condition (II, i) with various values of n and $\Omega_0 = 1$. For plane Poiseuille flow and with $n = 7$ the maximum value is 12, and for plane Couette flow and with $n = 3$ the maximum value of G is 4.8. In both cases, moderate transient growth is observed, with the maximum growth being lower than that obtained by Butler & Farrell (1992). For Couette flow, these authors have shown that the maximum optimal energy growth for this choice of $\tilde{\alpha}$ and ϕ occurs at $t = 8.7$. Here, we observe that the largest growth is for the initial condition with $n = 3$ and the maximum occurs at time $t = 7.8$. The same can be said of Poiseuille flow. Butler & Farrell have shown that the optimal initial conditions for Poiseuille flow produce a maximum at time $t = 14.1$ and the largest growth here is for $n = 7$ that has a maximum at time $t = 14.4$. It is easy to see how these solutions for different values of n can be combined to produce an optimal solution. This issue is explored further in §4.3.

4.2. *Three-dimensionality*

In this subsection results are presented for plane Poiseuille flow with $\tilde{\alpha} = 2.044$, $\phi = 90°$ and a Reynolds number of $Re = 5000$, and for plane Couette flow with $\tilde{\alpha} = 1.66$, $\phi = 90°$ and $Re = 1000$. These values are again those from Butler & Farrell
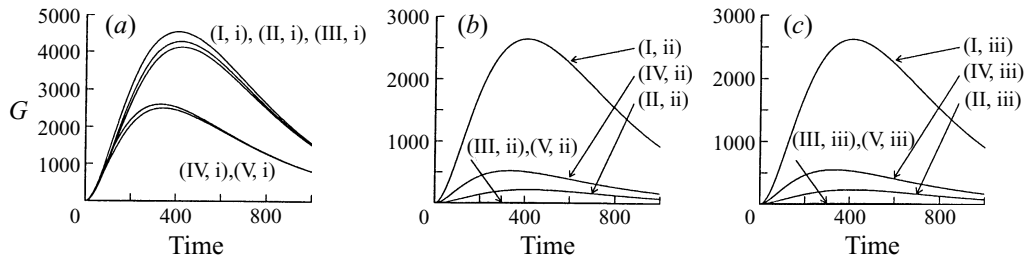
FIGURE 5. The growth function G as a function of time for various initial conditions. Results for plane Poiseuille flow with $\tilde{\alpha} = 2.044$, $\phi = 90°$, and $Re = 5000$.
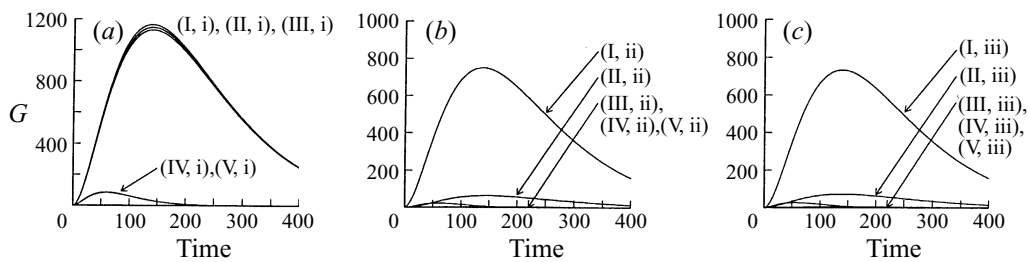

FIGURE 6. The growth function G as a function of time for various initial conditions. Results for plane Couette flow with $\tilde{\alpha} = 1.66$, $\phi = 90°$, and $Re = 1000$.

(1992) and the choice of $\tilde{\alpha}$ corresponds to the streamwise vortex with largest growth. In the case of plane Poiseuille flow the global optimal coincides with a streamwise vortex ($\phi = 90°$) but not so for Couette flow, where the global optimal was shown to be at $\phi \approx 88°$. In all calculations we set $\Omega_0 = \Omega_1 = \lambda = n = 1$. Changing the sign of Ω_1 produced only very minor changes in the solutions. Numerical experiments were also carried out for various combinations of n and λ with the largest value of G occurring for $n = \lambda = 1$. Therefore only this case is presented here.

The growth function is plotted as a function of time in figure 5 for plane Poiseuille flow and in figure 6 for plane Couette flow. The curves in (*a*) correspond to the initial condition (i) for $\tilde{w}$, the curves in (*b*) correspond to (ii) and the curves in (*c*) correspond to (iii). Comparing figures 3 and 5 for the case of plane Poiseuille flow, and figures 4 and 6 for the case of plane Couette flow, we see that the transient growth is significantly larger for three-dimensional disturbances than it is for two-dimensional disturbances. For plane Poiseuille flow, the maxima of the symmetric disturbances (labelled I, II, and III) and the maxima of the asymmetric disturbances (labelled IV and V) in figure 5(*a*) are within 90% of the global maxima reported by Butler & Farrell. They point out that the presence of streamwise vorticity, while passive to nonlinear dynamics (Gustavsson 1991), can cause the development of streaks which may themselves be unstable to secondary instabilities or possibly produce transient growth of other types of perturbations. For plane Couette flow, the maxima of the symmetric disturbances (labelled I, II, and III) in figure 6(*a*) are within 97% of the maxima reported by Butler & Farrell, while the maxima of the asymmetric disturbances (labelled IV and V) are significantly smaller. Thus, any initial condition with $\tilde{v}$-velocity symmetric and no initial vorticity will give near optimum results when three-dimensionality is considered. This easily explains the growth observed by Gustavsson when a limited normal mode initial condition was employed.
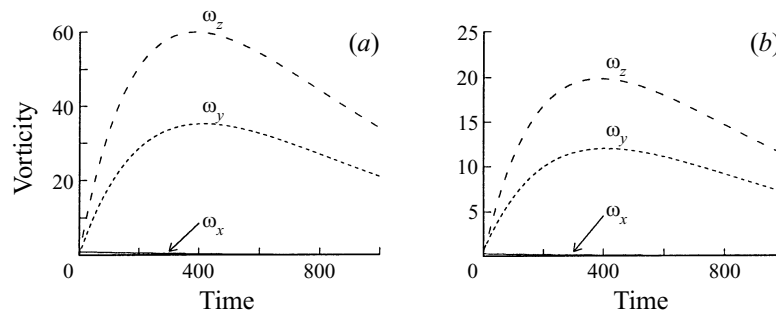
FIGURE 7. The vorticity components as a function of time for the initial conditions (*a*) (II, i) and (*b*) (II, ii). Results for plane Poiseuille flow with $\tilde{\alpha} = 2.044$, $\phi = 90°$, and $Re = 5000$.

Since this large transient growth for three-dimensional disturbances is a direct result of the growth of vorticity, it is necessary to ask whether the growth is a special case because the initial vorticity is neglected, or will the growth in energy remain once the energy of non-zero initial vorticity is included in the calculation. Note in figures 5 and 6 that the symmetric disturbances all behave in a similar manner when the initial condition for $\tilde{w}$ is given by (i), but differ substantially when conditions (ii) or (iii) are used. It is clear that the substantial growth in energies shown in figure 5(*a*) is directly attributable to the generation of normal vorticity through the coupling term in equation (13). This produces growth factors of 3900–4200 for symmetric initial profiles (I, II, and III) and growth factors of 2200–2400 for antisymmetric initial profiles (IV and V). The responses change significantly when the energy of the initial profiles (ii) and (iii) is included in the initial normalization of the growth factor *G*. The responses to initial profiles I and IV are lowered but still show significant growth. The initial energy of II and IV is larger than that of (ii) and (iii). However, when the energies of the initial normal vorticities (ii) and (iii) are significantly larger or comparable to the energies of the initial velocity profiles II, III, and V, the substantial transient growth as measured by the total energy can decrease by a factor of 10. This is not to say that the transient growth shown in (*a*) is not also present in (*b*) and (*c*), but that the normalization in (*b*) and (*c*) reflects a more proper measure of growth that includes the total energy of an arbitrarily chosen initial disturbance and not just an optimal one. This suggests that the algebraic growth as measured here and in previous work is extremely sensitive to the presence of any initial normal vorticity, specifically to the inclusion of its energy in the normalization of the growth factor. Vorticity components are presented in figure 7 for plane Poiseuille flow with initial conditions given by (II, i) and (II, ii), respectively, showing that the maxima in time of the normal and spanwise vorticity components decrease when the normal vorticity component is initially non-zero. The streamwise component decays and is unaffected by this change of initial conditions.

Finally, shown in tables 4(*a*) and 4(*b*) are the times (t^*) for which the growth function, *G*, attains its maximum (G^*) at various Reynolds numbers for plane Poiseuille and plane Couette flow, respectively. Note that the time scales as *Re* while the maximum scales as Re^2, as previously noted by Gustavsson (1991).

4.3. *Optimal initial conditions*

A mechanism for rapid transient growth when the initial condition is expressed as a sum of the eigenfunctions has been given by Reddy & Henningson (1993). The concept

	Re	t^*	G^*	t^*/Re	G^*/Re^2
(a)	500	41.0	45.6	0.0820	1.824×10^{-4}
	1000	82.0	181.9	0.0820	1.819×10^{-4}
	2000	164.0	726.9	0.0820	1.817×10^{-4}
	4000	327.0	2907.0	0.0818	1.817×10^{-4}
	5000	409.0	4542.0	0.0818	1.817×10^{-4}
(b)	500	69.0	291.4	0.1380	1.165×10^{-3}
	1000	139.0	1165.2	0.1390	1.165×10^{-3}
	2000	277.0	4660.7	0.1385	1.165×10^{-3}
	4000	554.0	18642.4	0.1385	1.165×10^{-3}
	8000	1109.0	74569.6	0.1386	1.165×10^{-3}

TABLE 4. Maximum values at various Re corresponding to the initial condition (I, i) for (a) plane Poiseuille flow with $\tilde{\alpha} = 2.044$ and $\phi = 90°$, and (b) plane Couette flow with $\tilde{\alpha} = 1.66$ and $\phi = 90°$.

is that a group of eigenfunctions are nearly linearly dependent so that, in order to represent an arbitrary disturbance (say), then it is possible that the coefficients can be quite large. Now, since each one of these nearly linearly dependent eigenfunctions has differing decay rates, the exact cancellations that produce the given initial disturbance might not persist in time and thus significant transient growth can occur. The mechanism can be (and is) taken a step further in order to determine the optimal initial condition (still expressed as a sum of the non-orthogonal eigenfunctions) that produces the largest relative energy growth for a certain time period. When this procedure is completed it can be seen to have the feature that the nearly linearly dependent eigenfunctions are multiplied by coefficients three orders of magnitude greater than the others. This optimal initial condition produces a growth factor of about 20 for the two-dimensional disturbance in Poiseuille flow. However, this optimal growth is nearly destroyed by not including the first eigenfunction (growth drops to a factor of 6 rather than 20) which seems to indicate that the prior explanation of (initial) exact cancellations by the nearly linearly dependent eigenfunctions is not the entire mechanism. Butler & Farrell (1992) also calculated optimal initial conditions in terms of a summation of the eigenfunctions (although they put no particular emphasis on the importance of using this approach) and reiterated the importance of near-linear dependence of the modes to the transient growth. This work also explained the transient growth of the optimal initial conditions in terms of the vortex-tilting mechanism and the Reynolds stress mechanism, since these (physical) arguments apply no matter what the solution method.

By the method that we have been following, an optimization procedure can be determined without resorting to a variational procedure. A closer inspection of initial condition II suggests that each of these disturbances is in essence a single Fourier mode of an arbitrary initial condition. If one were to consider an arbitrary odd function for the $\tilde{u}$-velocity satisfying the boundary conditions written in terms of a Fourier sine series, then the initial condition in the $\tilde{v}$-velocity is given by II. Thus, if one wished to determine an optimal initial disturbance, a maximization procedure could be applied to an arbitrary linear combination of these modes, all of which are initially orthogonal and linearly independent. Clearly, if one wanted to also include non-zero initial vorticity in such an optimization scheme it would not be difficult (and these initial conditions are of course very important when modelling real disturbances as opposed to optimal disturbances). The results presented here show that, if included
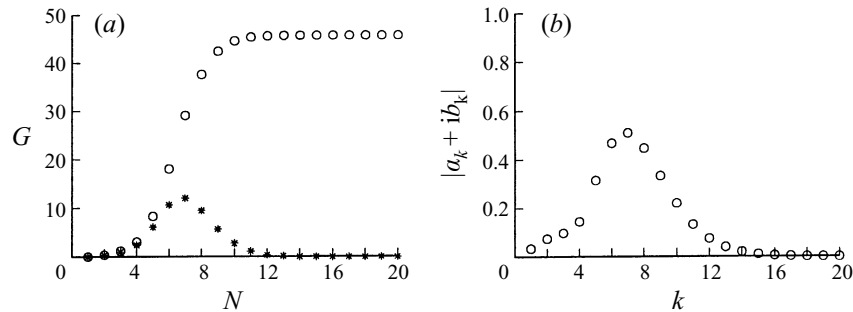
FIGURE 8. (*a*) The growth function G at $t = 14.1$; individual mode results denoted by $*$; cumulative results from optimization procedure denoted by $\circ$. (*b*) The magnitude of the coefficients $a_k + ib_k$ from optimization procedure for $N = 20$. For plane Poiseuille flow with $\tilde{\alpha} = 1.48$, $\phi = 0°$, and $Re = 5000$.

in the optimization procedure, the initial vorticity modes would not contribute to the optimal solution for the cases considered.

To start the optimization scheme, we consider the total solution $\boldsymbol{u} = (\breve{u}, \breve{v}, \breve{w})$ to be the sum

$$\boldsymbol{u}(y,t) = \sum_{k=1}^{N}(a_k + ib_k)\boldsymbol{u}_k(y,t),$$

where each of the vectors $\boldsymbol{u}_k(y,t)$ represents a solution to equations (12) and (13) subject to the initial conditions

$$\boldsymbol{u}(y,0) = \left\{ \begin{array}{c} \cos\phi\sin k\pi y \\ (i\tilde{\alpha}/k\pi)(\cos k\pi - \cos k\pi y) \\ \sin\phi\sin k\pi y \end{array} \right\}.$$

In order to maximize the growth function, it is sufficient to maximize the energy,

$$E(t) = \int_{-1}^{1} \boldsymbol{u}(y,t) \cdot \boldsymbol{u}^*(y,t)\,\mathrm{d}y,$$

subject to the constraint

$$E(0) = 1.$$

Therefore, we use Lagrange multipliers to maximize the function

$$\bar{G}(t) = \int_{-1}^{1} \boldsymbol{u}(y,t) \cdot \boldsymbol{u}^*(y,t)\,\mathrm{d}y - \lambda\left(\int_{-1}^{1} \boldsymbol{u}(y,0) \cdot \boldsymbol{u}^*(y,0)\,\mathrm{d}y - 1\right),$$

that requires

$$\frac{\partial\bar{G}}{\partial a_k} = 0, \qquad \frac{\partial\bar{G}}{\partial b_k} = 0, \qquad k = 1, 2, \ldots, N.$$

The set of equations thus derived produces a $2N \times 2N$ generalized eigenvalue problem. A search over the eigenvectors gives the initial condition with initial unit energy that maximizes the function $\bar{G}$ at time t.

To illustrate the optimization procedure, we perform the calculations for the two cases reported by Butler & Farrell (1992). The first is the computation of the two-dimensional optimal for $\tilde{\alpha} = 1.48$, $\phi = 0°$ and $Re = 5000$. In figure 8(*a*) we show the growth factor at $t = 14.1$ for each individual mode as well as for the optimal

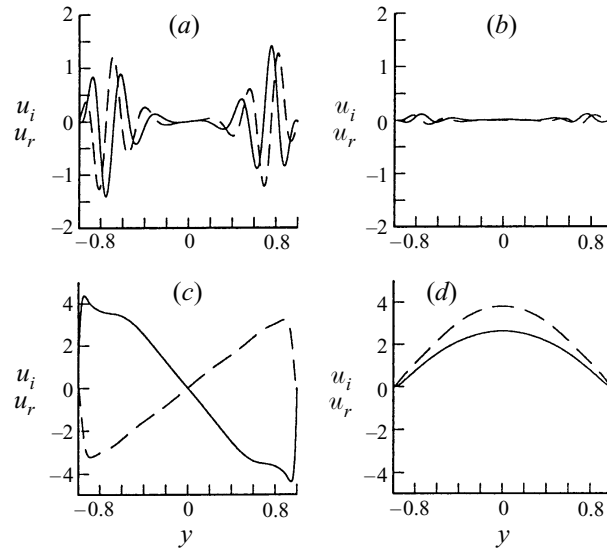*W. O. Criminale, T. L. Jackson, D. G. Lasseigne and R. D. Joslin*

FIGURE 9. Velocities for plane Poiseuille flow from optimization procedure with $N = 20$, $\tilde{\alpha} = 1.48$, $\phi = 0°$, and $Re = 5000$. (a) $\breve{u}_r$ (solid), $\breve{u}_i$ (dashed) at $t = 0$; (b) $\breve{v}_r$ (solid), $\breve{v}_i$ (dashed) at $t = 0$; (c) $\breve{u}_r$ (solid), $\breve{u}_i$ (dashed) at $t = 14.1$; (d) $\breve{v}_r$ (solid), $\breve{v}_i$ (dashed) at $t = 14.1$.

solution for various values of N. The convergence as $N \to \infty$ is nicely illustrated; compare with Reddy & Henningson (1993) for example. In figure 8(b) the magnitudes of the coefficients which produce the optimum with $N = 20$ are shown. There are no surprises. Each coefficient is of reasonable size, with the largest coefficient being a factor of 10 greater than the first coefficient, and not a factor of a 1000 as is the case when using eigenfunction expansions where a group of eigenfunctions is nearly linearly dependent and is not orthogonal. The magnitudes peak for $k = 6, 7$ and 8 which could be easily predicted from the previous graphs for the responses to each individual mode. For completeness the initial velocity profiles are shown in figure 9. These are consistent with the initial perturbation streamfunction contour plots shown in Butler & Farrell (1992). A similar calculation could be made for Couette flow but is unnecessary since the relevant information is easily determined by examination of figure 4(b). The magnitudes of the coefficients which produce the optimal growth at $t = 8.7$ peak between modes 3 and 4, and converge quickly as $N \to \infty$. The resulting initial condition is consistent with the initial perturbation streamfunction contour plots shown by Butler & Farrell for the same case. The second calculation is for the optimal three-dimensional disturbance. The parameters chosen are $Re = 5000$, $\tilde{\alpha} = 2.044$ and $\phi = 90°$. The initial conditions that produce a maximum growth at $t = 379$ are found. The results are shown in figure 10, and the composition of the initial conditions in terms of the modes chosen here could be easily determined from the individual responses of each mode.

It must be reiterated that, although it is possible and conceptually easy to reproduce the optimal initial conditions that have been previously found, the maximum transient growth is only a measure of what is possible and not what will actually occur as has been the difficulty in devising experiments. It is at least as important to investigate whether such large growth is possible for arbitrary initial conditions. In this regard, the results presented here produce a mostly negative answer to this question. For two-dimensional disturbances in Poiseuille flow, the transient growth observed for
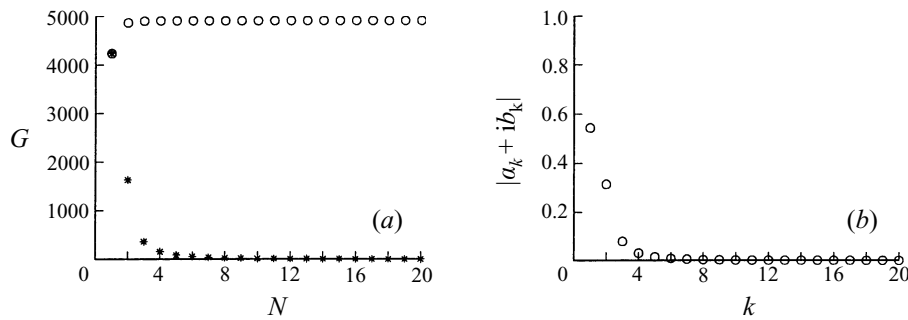
FIGURE 10. (a) The growth function G at $t = 379.0$; individual mode results denoted by $*$; cumulative results from optimization procedure denoted by $\circ$. (b) The magnitude of the coefficients $a_k + ib_k$ from optimization procedure for $N = 20$. For plane Poiseuille flow with $\tilde{\alpha} = 2.044$, $\phi = 90°$, and $Re = 5000$.

arbitrarily chosen initial conditions using this approach is, at best, only 25% of the optimal. When considering a fixed wavelength $\tilde{\alpha}$ and a fixed obliqueness ϕ, it is seen that very large relative energy growth of the perturbation can be observed in Poiseuille flow for oblique disturbances with arbitrary velocity profiles restricted to having zero initial normal vorticity, but the relative energy growth quickly decreases when arbitrary disturbances are combined with initial normal vorticity. Similar results are found for Couette flow.

5. Direct numerical simulation

In this section we compare the theoretical results developed for the temporal problem to spatial direct numerical simulation (DNS) calculations. First, the numerical techniques required for the simulation and the inflow condition are briefly discussed. For a detailed description of the spatial DNS (Navier–Stokes) approach used, refer to Joslin, Streett & Chang (1992, 1993).

The instantaneous velocities $\tilde{\boldsymbol{u}} = (\tilde{u}, \tilde{v}, \tilde{w})$ and the pressure $\tilde{p}$ are decomposed into steady base and disturbance components. The base flow is given by velocities $\boldsymbol{U} = (U, V, W)$ and the pressure P; the disturbance is given by velocities $\boldsymbol{u} = (u, v, w)$ and the pressure p. The velocities correspond to the coordinate system $\boldsymbol{x} = (x, y, z)$, where x is the streamwise direction, y is the wall-normal direction, and z is the spanwise direction. The base flow is taken to be the Poiseuille flow with $\boldsymbol{U} = (U(y), 0, 0)$ and the disturbance flow is found by solving the three-dimensional, incompressible Navier–Stokes equations. These equations are the momentum

$$\boldsymbol{u}_t + (\boldsymbol{u} \cdot \nabla)\boldsymbol{u} + (\boldsymbol{U} \cdot \nabla)\boldsymbol{u} + (\boldsymbol{u} \cdot \nabla)\boldsymbol{u} = -\nabla p + \frac{1}{Re}\nabla^2\boldsymbol{u} \tag{22}$$

and continuity

$$\nabla \cdot \boldsymbol{u} = 0 \tag{23}$$

equations, respectively. The boundary conditions at the wall are

$$\boldsymbol{u} = 0 \quad \text{at} \quad y = \pm 1, \tag{24}$$

plus an appropriate inflow condition at $x = 0$.

To solve the above equations computationally, the spatial discretization entails a Chebyshev collocation grid in the wall-normal direction, fourth-order finite differences for the pressure equation, sixth-order compact differences for the momentum
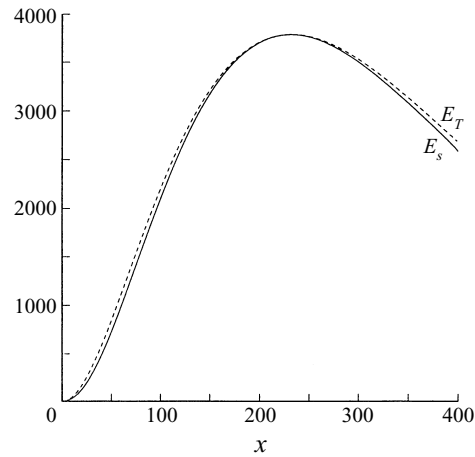
FIGURE 11. The normalized energy E_s as a function of streamwise distance x at $Re = 5000$. Also shown as a dashed line is the normalized energy E_T from the temporal solutions scaled in such a way that both the amplitude and location coincide at the maximum, i.e. $x = 0.561t$ and $E_T = 0.831E(t)$.

equations in the streamwise direction, and a Fourier sine and cosine series in the spanwise direction on a staggered grid (Joslin *et al.* 1993). For time marching, a time splitting procedure is used with implicit Crank–Nicolson differencing for normal diffusion terms and an explicit three-stage Runge–Kutta method (Williamson 1980). The influence matrix technique is employed to solve the resulting pressure equation (Helmholtz–Neumann problem) (Streett & Hussaini 1991; Danabasoglu, Biringen & Streett 1991). At the outflow, the buffer domain technique of Streett & Macaraeg (1989) is used. A grid resolution study was performed, and the results presented below represent converged solutions. On the finest mesh, these three-dimensional calculations took about 20 hours of CPU time on the Cray-YMP.

The inflow conditions have been chosen to correspond with the appropriate initial condition (I,i) with $\alpha = 0$ and $\gamma = 2$, i.e.

$$\boldsymbol{u} = \epsilon \left(0, (1 - y^2)^2 \cos(2z), 2y(1 - y^2) \sin(2z)\right) \tag{25}$$

where ϵ is the initial amplitude taken here to be 10^{-7} such that the transient disturbance remains small so that comparisons with linear theory can be made. This inflow condition corresponds to near optimal growth for the temporal problem at the subcritical Reynolds number of $Re = 5000$. The numerical code was run for sufficient time such that steady state has been achieved in a region which includes all of the relevant spatial growth. In figure 11 we plot the normalized energy E_s as a function of streamwise distance x, calculated at steady state. As suggested from temporal theory, for this subcritical Reynolds number case, there is significant transient growth and subsequent decay. Also shown in this figure as a dashed line is the normalized energy E_T from the temporal solutions scaled in such a way that both the amplitude and location coincide at the maximum. The temporal results are obtained by solving equations (12) and (13) subject to the initial conditions given by (25). The temporal results were scaled as follows:

$$x = 0.561t, \qquad E_T = \frac{3783.71}{4551.94} E(t) = 0.831E(t). \tag{26}$$

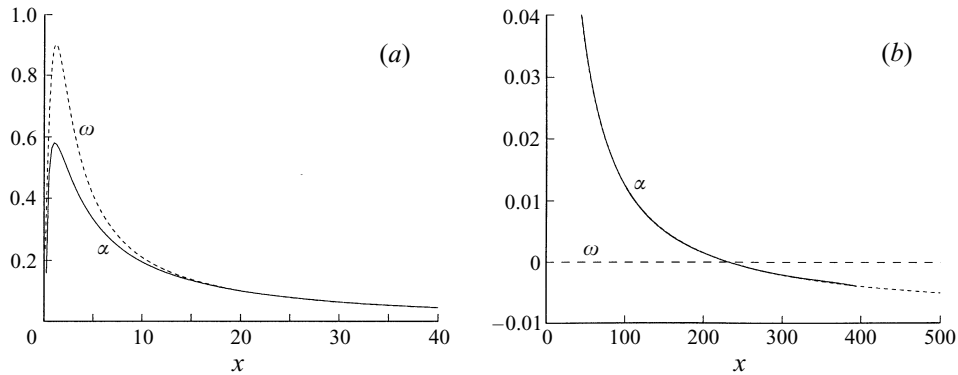As can be seen, there is considerable agreement between the two, hinting at the

FIGURE 12. The spatial (solid) and temporal (dash) growth rates as a function of x. Graph (a) shows the region $0 \leqslant x \leqslant 40$ while (b) shows the region $0 \leqslant x \leqslant 500$. Using the previous relationship between x and t, the growth rates are identically zero at the same value of x. The temporal growth rate ω is further scaled by 2.

possibility of a spatial–temporal transformation. Further insight into such a possible connection is explored in figure 12 where we plot the growth rates as a function of x. The growth rates for both the spatial and temporal solutions are defined in the following manner:

$$\frac{1}{E_s}\frac{\mathrm{d}E_s}{\mathrm{d}x} = \alpha(x), \qquad \frac{1}{E(t)}\frac{\mathrm{d}E(t)}{\mathrm{d}t} = \omega(t). \qquad (27)$$

Using the previous relationship between x and t, the growth rates are identically zero at the same value of x. A further scaling of ω by a factor of 2 suggests that a relationship of the form

$$\alpha(x) = \frac{\omega(x/0.561)}{c}, \qquad c = \tfrac{1}{2}, \qquad (28)$$

holds over most of the domain except for the very early transients. This value of c corresponds to half of the channel velocity. In the absence of a theory connecting spatial and temporal calculations, these results prove to be very interesting and suggest an area of further study. If a spatial–temporal relationship could be determined, then the temporal theory could be used to study the spatial problem at a fraction of the cost of a DNS study.

6. Conclusions

Plane Poiseuille and plane Couette flows in an incompressible viscous fluid have been investigated subject to the influence of small perturbations. In lieu of using the techniques of classical stability analysis or the more recent techniques involving eigenfunction expansions, the approach here has been to first Fourier transform the governing disturbance equations in the streamwise and spanwise directions only and then solve the resulting partial differential equations numerically by the method of lines. Unlike traditional methods where travelling wave normal modes are assumed for solution, this approach offers another means whereby arbitrary initial input can be specified. Thus, arbitrary initial conditions can be imposed and the full temporal behaviour, including both early-time transients and the long-time asymptotics, can be determined. All of the stability data that are known for such flows can be

reproduced. In addition, an optimization scheme is presented using the orthogonal Fourier series and all previous results using variational techniques and eigenfunction expansions are reproduced. However, it is shown here that the transient growth of the perturbation energy density is very sensitive to the presence of an initial normal vorticity perturbation. Finally, direct numerical simulation of the spatial problem is carried out and compared with the linear temporal theory. In the absence of a theory connecting spatial and temporal calculations, these results prove to be very interesting and suggest an area of further study.

The benefit of this approach is clear for it can be applied to other classes of problems where only a finite number of normal modes exist, such as the Blasius boundary layer. In addition, this numerical approach has recently been successfully applied to free shear flows in an inviscid fluid (Criminale *et al.* 1995). These concepts are being extended to the Blasius boundary layer in both an incompressible and compressible medium.

REFERENCES

AMES, W. F. 1977 *Numerical Methods for Partial Differential Equations*. Academic Press.

BENNEY, D. J. & GUSTAVSSON, L. H. 1981 A new mechanism for linear and nonlinear hydrodynamic instability. *Stud. Appl. Maths* **64**, 185–209.

BETCHOV, R. & CRIMINALE, W. O. 1967 *Stability of Parallel Flows*. Academic Press.

BOBERG, L. & BROSA, U. 1988 Onset of turbulence in a pipe. *Z. Naturferschung* **43a**, 697–726.

BRUER, K. S. & KURAISHI, T. 1994 Transient growth in two- and three-dimensional boundary layers. *Phys. Fluids* **6**, 1983–1993.

BUTLER, K. M. & FARRELL, B. F. 1992 Three-dimensional optimal perturbations in viscous shear flow. *Phys. Fluids* A **4**, 1637–1650.

BUTLER, K. M. & FARRELL, B. F. 1994 Nonlinear equilibration of two-dimensional optimal perturbations in viscous shear flow. *Phys. Fluids* A **6**, 2011–2020.

CASE, K. M. 1960 Stability of inviscid plane Couette flow. *Phys. Fluids* **3**, 143–148.

CRIMINALE, W. O. & DRAZIN, P. G. 1990 The evolution of linearized perturbations of parallel flows. *Stud. Appl. Maths* **83**, 123–157.

CRIMINALE, W. O., JACKSON, T. L. & LASSEIGNE, D. G. 1995 Towards enhancing and delaying disturbances in free shear flows. *J. Fluid Mech.* **294**, 283–300.

DANABASOGLU, G., BIRINGEN, S. & STREETT, C. L. 1991 Spatial simulation of instability control by periodic suction and blowing. *Phys. Fluids* **3**, 2138–2147.

DIPRIMA, R. C. & HABETLER, G. J. 1969 A completeness theorem for non-selfadjoint eigenvalue problems in hydrodynamic stability. *Arch. Rat. Mech. Anal.* **34**, 218–227.

DRAZIN, P. G. & REID, W. H. 1981 *Hydrodynamic Stability*. Cambridge University Press.

FARRELL, B. F. 1988 Optimal excitation of perturbations in viscous shear flow. *Phys. Fluids* **31**, 2093–2102.

FARRELL, B. F. & MOORE, A. M. 1992 An adjoint method of obtaining the most rapidly growing perturbation to oceanic flows. *J. Phys. Oceanogr.* **22**, 338–349.

GROSCH, C. E. & SALWEN, H. 1978 The continuous spectrum of the Orr–Sommerfeld equation. Part 1. The spectrum and the eigenfunctions. *J. Fluid Mech.* **87**, 33–54.

GUSTAVSSON, L. H. 1979 Initial-value problem for boundary layer flows. *Phys. Fluids* **22**, 1602–1605.

GUSTAVSSON, L. H. 1991 Energy growth of three-dimensional disturbances in plane Poiseuille flow. *J. Fluid Mech.* **224**, 241–260.

HERRON, I. H. 1980 A completeness observation on the stability equations for stratified viscous shear flows. *Phys. Fluids* **23**, 836–837.

HULTGREN, L. S. & GUSTAVSSON, L. H. 1980 Algebraic growth of disturbances in a laminar boundary layer. *Phys. Fluids* **24**, 1000–1004.

JOSLIN, R. D., STREETT. C. L. & CHANG, C. L. 1992 Validation of three-dimensional incompressible spatial direct numerical simulation code – A comparison with linear stability and parabolic stability equations theories for boundary-layer transition on a flat plate. *NASA TP*-3205.

JOSLIN, R. D., STREETT. C. L. & CHANG, C. L. 1993 Spatial direct numerical simulation of boundary-layer transition mechanisms: validation of PSE theory. *Theor. Comput. Fluid Dyn.* **4**, 271–288.

KELVIN, LORD 1887 Stability of fluid motion – Rectilinear motion of viscous fluid between two parallel planes. *Phil. Mag.* **24**, 188–196.

MACK, L. M. 1976 A numerical study of the temporal eigenvalue spectrum of the Blasius boundary layer. *J. Fluid Mech.* **73**, 497–520.

ORR, W. M'F. 1907a The stability or instability of the steady motions of a perfect liquid and a viscous liquid. Part I. *Proc. R. Irish. Acad.* **27**, 9–68.

ORR, W. M'F. 1907b The stability or instability of the steady motions of a perfect liquid and a viscous liquid. Part II. *Proc. R. Irish. Acad.* **27**, 69–138.

ORSZAG, S. A. 1971 Accurate solution of the Orr–Sommerfeld equation. *J. Fluid Mech.* **50**, 689–703.

REDDY, S. C. & HENNINGSON, D. S. 1993 Energy growth in viscous channel flows. *J. Fluid Mech.* **252**, 209–238.

SALWEN, H. & GROSCH, C. E. 1981 The continuous spectrum of the Orr–Sommerfeld equation. Part 2. Eigenfunction expansions. *J. Fluid Mech.* **104**, 445–465.

SCHENSTED, I. V. 1960 Contributions to the theory of hydrodynamic stability. PhD dissertation, University of Michigan.

SOMMERFELD, A. 1949 *Partial Differential Equations in Physics*. Lectures in Theoretical Physics, Vol. 6. Academic Press.

STREETT, C. L. & HUSSAINI, M. Y. 1991 A numerical simulation of the appearance of chaos in finite-length Taylor-Couette flow. *Appl. Numer. Maths* **7**, 41–71.

STREETT, C. L. & MACARAEG, M. G. 1989 Spectral multi-domain for large-scale fluid dynamic simulations. *Intl J. Appl. Numer. Maths* **6**, 123–140.

TREFETHEN, L. N., TREFETHEN, A. E., REDDY, S. C. & DRISCOLL, T. A. 1993 Hydrodynamic stability without eigenvalues. *Science* **261**, 578.

WILLIAMSON, J. H. 1980 Low-storage Runge–Kutta schemes. *J. Comput. Phys.* **35**, 48–56.